Electromagnetic Cavity Resonance Equalization with Bandpass Negative Group Delay

Blaise Ravelo, Sébastien Lalléchère, Wenceslas Rahajandraibe, Fayu Wan

Electromagnetic Cavity Resonance Equalization with Bandpass Negative Group Delay

Blaise Ravelo, *Member, IEEE*, Sébastien Lalléchère, *Member, IEEE*, Wenceslas Rahajandraibe, *Member, IEEE* and Fayu Wan, *Member, IEEE*

***Abstract*—This paper deals with an original equalization method of 3-D electromagnetic (EM) cavity resonance by using bandpass negative group delay (NGD) function. Based on the equivalent circuit, the S-matrix model of the equalized EM cavity is introduced. The design equations of the NGD function are established in function of the cavity physical parameters. The feasibility of the equalization method is validated with a 42×28×3.8 cm rectangular cavity containing two communicating monopole antennas. By considering the TE110-mode, a significant equalization is realized with improvement of transmission coefficient flatness from 4-dB to less than 0.3-dB. In addition to the magnitude, the NGD equalization method enables to outstandingly reduce spikes of 3-D EM cavity group delay. With the proof of concept, the GD is reduced from more than 4-ns into 1-ns.**

***Index Terms*—Bandpass negative group delay (NGD), 3-D Electromagnetic cavity, EMI, Equalization method, Equivalent circuit, Synthesis equation.**

I. Introduction

THE performances of modern electronic and communication devices suffer from unintentional radiated electromagnetic interreferences (EMIs) [1-7]. The interference issues were found at different scale of electronic systems. For example, the wireless system quality of services is frequently victim of propagation channel multipaths [1], cyclic delay [2] and group delay (GD) mitigation [3]. The EMI effects were emphasized in different systems as medical equipment's [4-6].

More frequently, EMI effects decrease printed circuit board (PCB) performances due to the enclosure cavity resonances [7-8]. The characterization of metallic cavity resonances [9-10] by using TEM cells is one of the most attractive activities of electromagnetic compatibility (EMC) research engineers. But because of the EMC characterization test costs, during the two last decades more and more modelling and simulation approaches of metallic enclosure EM resonances were developed [11-27]. The successful popularity of computer-aided design tools favors the development of algorithmic and iterative solvers for the modelling of EM cavities [11-13]. The emergence of circuit and 3-D EM full wave commercial tools [14-19] was helpful for the EMC engineers to simulate certain EMC effects as the cavity-based structures. However, the simulation results of commercial tools are not always easy to interpret for many engineer users. Therefore, EMC cavity effect analytical formulations [20-29] were developed in parallel for the mathematical understanding of EMC performances. Different approaches were suggested for the modelling of EM shielding for example by using coupling with metallic wires [21] or by placing a receiver antenna [22, 29] enclosed in the cavity. So far, these modelling methods enable to predict with significant accuracy the EM field inside the shielding enclosure under computation speed generally faster than the commercial tools and/or measurements.

Nevertheless, most of enclosure EMC problems cannot be completely solved with the simulators despite the success of popular full wave commercial tools [15-19]. To face up the issues related to the EMC resonances emanated by cavity enclosures, few tentative techniques of resonance suppression were initiated in [30-32]. An improvement of shielding effectiveness was presented in [30] by using a coating well structure. An introduction technique of lossy resonators is proposed in [31] to suppress the PCB power bus resonance. Then, a PCB EMI reduction technique was developed [32] by using EM bandgap structures. However, those resonance suppression techniques are limited to very narrow bandwidth and requires quite expensive design and fabrication of shielding structures. Furthermore, the mechanism of these techniques is particularly hard to translate analytically.

To overcome these limitation challenges, a completely original technique of 3-D EM cavity resonance effect by using the unfamiliar bandpass negative group delay (NGD) function is initiated in the present paper. The basic principle of NGD equalization based on the cascading with positive group delay (PGD) circuit as a transmission line (TL) was introduced briefly in [33-35]. The algebraic principle is ideally the addition of PGD and NGD that should generate GD equal to zero. The

Manuscript received xxx xx, 2020; revised xxx xx, 2020; accepted xxx xx, 2020. Date of publication xxx xx, 2020.

This research work was supported in part by NSFC under Grant 61601233 and Grant 61971230, in part by the Electrostatic Research Foundation of Liu Shanghe Academicians and Experts Workstation, Beijing Orient Institute of Measurement and Test under Grant BOIMTLSHJD20181003, in part by the Jiangsu Innovation and Enterprise Group Talents Plan 2015 under Grant SRCB201526, and in part by The Priority Academic Program Development of Jiangsu Higher Education Institutions.

Blaise Ravelo and Fayu Wan are with School of Electronic & Information Engineering, Nanjing University of Information Science & Technology (NUIST), Nanjing, Jiangsu 210044, China (e-mail: blaise.ravelo@nuist.edu.cn, Corresponding author e-mail: fayu.wan@nuist.edu.cn).

Sébastien Lalléchère is with the Université Clermont Auvergne (UCA), CNRS, SIGMA Clermont, Institut Pascal, Aubière, France. (email: sebastien.lallechere@uca.fr).

Wenceslas Rahajandraibe is with the Aix-Marseille University, CNRS, University of Toulon, IM2NP UMR7334, Marseille, France (e-mail: wenceslas.rahajandraibe@im2np.fr).

NGD equalization method was exploited to design a broadband phase shifter with constant phase independently to the frequency [34], for compensation of microwave oscillators and filters [35], for expansion of bandwidth of tunable dispersion compensator based on ring resonators [36], and to design equal-ripple filter [37]. A typical signal integrity exploitation of the NGD equalization technique was proposed in [38] to neutralize the RC- and LC-interconnect effects. But, so far, such a type of NGD application is strictly limited to planar RF and microwave circuits. In other word, in the best of the authors knowledge, because of its counterintuitive interpretation, the NGD function remains an unfamiliar concept for EMC engineers and no application is invoked. To break this roadblock, we expect that the unfamiliar NGD function should be a good candidate against EMC problems as the cavity resonance effect. Before the elaboration of this original idea, it is worth to describe quickly a recent state of the art on the bandpass NGD function.

Recent studies confirm the feasibility of the NGD microstrip and lumped circuit designs [39-44]. With passive circuit, the apparition of NGD effect is naturally accompanied by absorption [39] and/or reflection. To face up this constraint, challenging design of low-attenuation NGD circuits [40] was achieved. In addition to loss reduction, compact NGD circuits were also designed [40-41]. In contrary to the recursive questions about the existence of NGD topologies, the NGD function can be generated with any diverse electronic circuits, as presented in [42], by means of interference technique, an NGD circuit was proposed. To compensate the losses, active NGD circuits, for example, based on field effect transistor (FET) is proposed in [43]. Despite this progressive design, the NGD function remains an unfamiliar aspect for most of EMC engineers and requires further illustration for the basic understanding. In this way, an alternative approach illustrating the analogy between the NGD and filter functions was proposed in [44]. Depending on the NGD frequency band positioning, the concept of low-pass and bandpass NGD functions was introduced [44]. In the present paper, we are exploiting the bandpass NGD function to deal with the cavity EM resonance.

The paper is organized in four main sections. Section II introduces the basic principle of the resonance effect equalization by means of S-matrix modelling of linear time-invariant (LTI) system. Section III develops the analytical equations of the cavity resonance suppression with bandpass NGD function. The design and synthesis equations of the NGD equalizer are established with respect to the resonator circuit parameters. Section IV is focused on the validation results. Then, Section V is the final conclusion.

II. Analytical Theory of 3-D EM Cavity Resonance Suppression

This section describes the analytical mechanism of 3-D EM resonance suppression. After the specification of resonant system, the equations for calculating the bandpass NGD circuit parameters will be established.

A. Formulation of Cavity Resonance Problem

The cavity EM resonance effects was investigated regularly by electronic engineers with metallic cavity enclosures [7-14, 20-32]. To represent the resonance problem, we consider the rectangular metallic enclosure inspired from the demonstrator introduced in [22]. This enclosure is assumed defined by dimensions (L_x,L_y,L_z) containing two-monopole antennas with physical lengths d_1 which are placed at $M_1(x_1,y_1=L_y/2,0)$ and $M_2(d+x_1,y_1,0)$. These two antenna terminals are supposed connected to two-port vector network analyzer (VNA) for S-parameter extraction:

$$[S^{EMI}(j\omega)] = \begin{bmatrix} S_{11}^{EMI}(j\omega) & S_{12}^{EMI}(j\omega) \\ S_{21}^{EMI}(j\omega) & S_{22}^{EMI}(j\omega) \end{bmatrix} \quad (1)$$

with $j\omega$ the complex angular frequency variable and the angular frequency variable $\omega = 2\pi f$. This metallic cavity is connected to the reference ground of the VNA. We assume that the monopole antennas are not connected to the cavity, they are linked to ports ❶ and ❷.

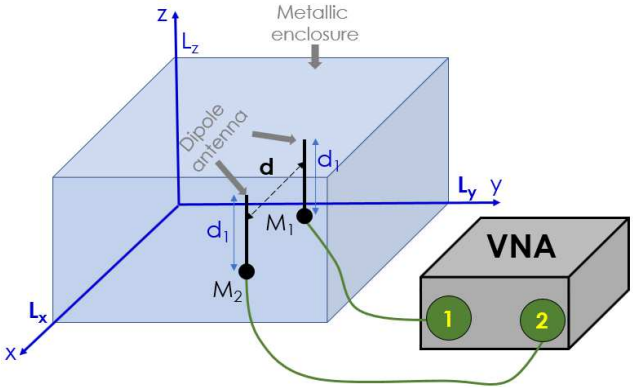

Fig. 1. Scenario of metallic enclosure with two communicating dipole antennas.

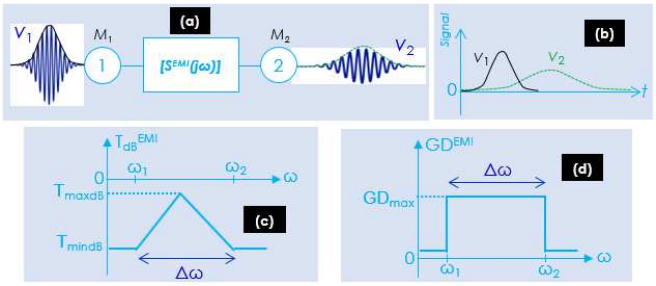

Fig. 2. Resonant system: (a) transient and (b) envelope responses, and TF (c) magnitude and (d) GD.

Fig. 2(a) illustrates a black box response of the resonant enclosure. As result of EM resonance, the output v_2 undergoes spreading effect compared to corresponding input v_1, as illustrated by the increase of envelope pulse width as depicted in Fig. 2(b). By taking $V_1(j\omega)$ and $V_2(j\omega)$ the spectra of signals at points M_1 and M_2, referred as ports ❶ and ❷, respectively, the resonant cavity transfer function (TF) can be defined by:

$$T^{EMI}(j\omega) = V_2(j\omega)/V_1(j\omega) \quad (2)$$

with the magnitude and phase written as:

$$\begin{cases} T^{EMI}(\omega) = \left| T^{EMI}(j\omega) \right| \\ \varphi^{EMI}(\omega) = \arg\left[T^{EMI}(j\omega) \right] \end{cases}. \quad (3)$$

The associated GD is analytically defined by:

$$GD^{EMI}(\omega) = -\partial\varphi^{EMI}(\omega)/\partial\omega. \quad (4)$$

To analyze the cavity resonance response, the TF system is assumed to operate in the frequency band with center $f_0 = \omega_0/(2\pi)$ over bandwidth $\Delta f = \Delta\omega/(2\pi)$ defined by:

$$\Delta\omega = \omega_2 - \omega_1 \quad (5)$$

with:

$$T_{\min} = \left| T^{EMI}(j\omega_1) \right| = \left| T^{EMI}(j\omega_2) \right|. \quad (6)$$

For example, at ω_0, the dispersion system TF present the magnitude $T_{\max} = T^{EMI}(\omega_0) = \left| T^{EMI}(j\omega_0) \right|$ and GD $GD_{\max} = GD^{EMI}(\omega_0)$. The resonance problem can be graphically illustrated by typical "Λ" shape curve of magnitude and GD behavior shown in Fig. 2(c) and Fig. 2(d), respectively.

B. Topological Solution of the Cavity Resonance Problem

The principle of the BP NGD equalization of the previously introduced 3-D EM cavity will be described in the following paragraph.

1) S-Matrix Description of the Cavity Effect Equalization

Fig. 3 gives an overview of the problem statement, considering free-space antennas communication (Fig. 3(a)), presence of a cavity (Fig. 3(b)), and use of BP NGD system (Fig. 3(c)). Thus, Fig. 3(a) depicts the block diagram of the dipole antennas communicating in free-air. The dipoles can be assumed as a two-port system connected to ports ❶ and ❷.

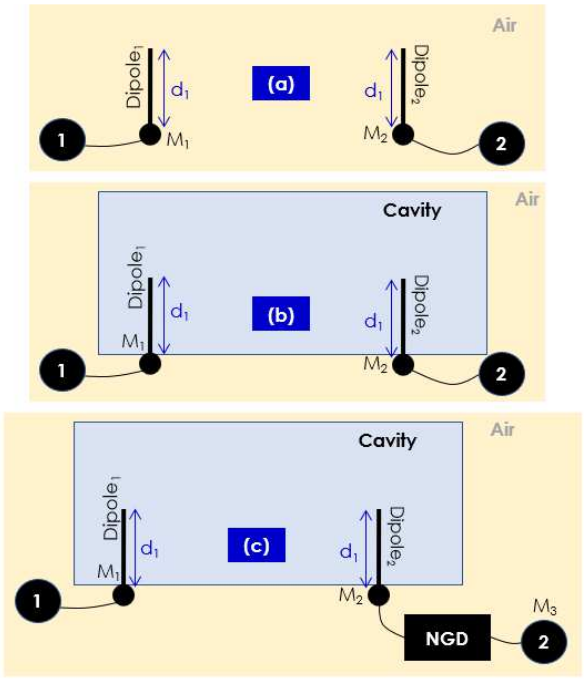

Fig. 3. Block diagram description of two-dipole antenna in (a) free-air, (b) inside a 3-D rectangular cavity and (c) in the cavity and dipole$_2$ connected to NGD circuit.

In the frequency band $[\omega_1, \omega_2]$ defined in Figs. 2(c) and 2(d), this reference system can be modelled with S-matrix:

$$\left[S^{air}(j\omega) \right] \approx \begin{bmatrix} 0 & \xi \\ \xi & 0 \end{bmatrix} \quad (7)$$

with ξ is the transmission loss assumed to be constant and frequency independent. With well-matched antennas placed inside the cavity as shown in Fig. 3(b), we can consider that the resonant system is equivalent to the S-matrix:

$$\left[S^{EMI}(j\omega) \right] = \begin{bmatrix} S_{11}^{EMI}(j\omega) & S_{21}^{EMI}(j\omega) \\ S_{21}^{EMI}(j\omega) & S_{11}^{EMI}(j\omega) \end{bmatrix}. \quad (8)$$

The main problem of the present study is to find a topological solution allowing to generate S-matrix, in the frequency band $[\omega_1, \omega_2]$:

$$\left[S^{eq}(j\omega) \right] = \begin{bmatrix} S_{11}^{eq}(j\omega) & S_{12}^{eq}(j\omega) \\ S_{21}^{eq}(j\omega) & S_{22}^{eq}(j\omega) \end{bmatrix} \quad (9)$$

with reflection and isolation coefficients:

$$S_{11,12,22}^{eq}(j\omega) \approx 0 \quad (10)$$

and transmission coefficient independent to frequency:

$$S_{21}^{eq}(j\omega) \approx 1. \quad (11)$$

We emphasize that:

- The term isolation coefficient here, is related to the use of unilateral active circuit, for example, using FET. In the ideal case of such circuit, S_{12} is close to zero.
- The justification of relation (11) is due to the fact that we want to restitute the distorted signal in order to generate an output as similar as possible to the corresponding input.

2) Justification of Bandpass NGD Function Equalizer Against the EMI Effect

The proposed analytical solution consists analytically in identifying an equalizer transmission coefficient $S_{21}^{?}(j\omega)$ (the symbol "?" standing for the searched term) allowing to realize the operation:

$$S_{21}^{eq}(j\omega) = S_{21}^{EMI}(j\omega) \times S_{21}^{?}(j\omega) \quad (12)$$

By supposing the equalized transmission coefficient of equation (11), we can derive the solution of previous equation:

$$S_{21}^{?}(j\omega) \approx 1/S_{21}^{EMI}(j\omega). \quad (13)$$

This unknown S-matrix can be identified by considering the resonant characteristic of the cavity responses introduced in Figs. 2(c) and 2(d). Therefore, the corresponding magnitude and GD must verify, respectively:

$$\left| S_{21}^{?}(j\omega) \right| \approx 1/\left| S_{21}^{EMI}(j\omega) \right| > 1 \quad (14)$$

$$GD^{?}(\omega) = \frac{-\partial \arg\left[S_{21}^{?}(j\omega) \right]}{\partial\omega} \approx -GD^{EMI}(\omega) < 0. \quad (15)$$

This last equation explains that the unknown system solution operates with NGD function. For this reason, the topological solution of block diagram illustrated in Fig. 3(c) is developed in the present paper. However, it is noteworthy that by adopting solution implemented with equation (15), the phase, $\varphi_{21}^{eq}(\omega) = \arg\left[S_{21}^{eq}(j\omega) \right]$, is not equal to zero. However, in this case, we still can realize the equalization when the magnitude and GD of the EMI effect are reduced to be closed to zero. In general, the NGD S-matrix can be written as:

$$\left[S^{?}(j\omega)\right]=\left[S^{N}(j\omega)\right]=\begin{bmatrix}S_{11}^{N}(j\omega) & S_{21}^{N}(j\omega)\\ S_{21}^{N}(j\omega) & S_{11}^{N}(j\omega)\end{bmatrix}. \quad (16)$$

This topological solution expects to operate with best results if ports ❶ and ❷ are well-matched:

$$\begin{cases}S_{11}^{EMI}(j\omega)=S_{22}^{EMI}(j\omega)<<1\\ S_{11}^{N}(j\omega)=S_{22}^{N}(j\omega)<<1\end{cases}. \quad (17)$$

3) Specifications of Bandpass NGD Function

As initiated in [44], a bandpass NGD function is specified by:

- The NGD center frequency, $f_n=\omega_n/(2\pi)$,
- The NGD value, $GD_n^N=GD^N(\omega_n)=\min\left[GD^N(\omega)\right]<0$,
- And the NGD bandwidth $BW_n=\omega_2^N-\omega_1^N$ which is associated to the cut-off angular frequencies $\omega_{1,2}^N$ represented by the root of equation:

$$GD^N(\omega_{1,2}^N)=0. \quad (18)$$

As reported in [39], the bandpass NGD function behaves similar to the bandpass filter but the analysis is not relying on the gain. We must focus on the behavior of:

$$GD^N(\omega)=\frac{-\partial\arg\left[S_{21}^N(j\omega)\right]}{\partial\omega}. \quad (19)$$

In graphical representation, the BP NGD responses related to the magnitude and GD behave generally as ideal curves as sketched in Fig. 4(a) and Fig. 4(b) by taking $T_{dB}^N(\omega)=20\log\left[S_{21}^N(j\omega)\right]$.

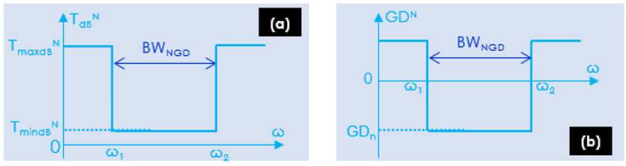

Fig. 4. NGD TF (a) magnitude and (b) GD responses.

III. NGD Design Equations From Equivalent Circuit Analysis

Based on the general solution evoked in the previous section, design equations of the NGD circuit are established in function of the cavity structure parameters.

A. Equivalent Circuit Description

For the sake of analytical simplicity and better understanding, we adopt the following hypotheses:

- The internal impedances of dipole$_1$ and dipole$_2$ are neglected,
- Only one of TE$_{mn}$ or TM$_{mn}$ propagative modes is considered,
- And the FET equivalent circuit is constituted by its transconductance g_m and drain-source resistance R_{ds}.

The proposed assumptions are relevant with the current work. First, the antennas internal impedances are weak considering Hertzian dipole, compliant with the equivalent circuit model [45] used in this work. Then, for the sake of simplicity, the methodology is presented with a unique propagative mode. These results might be extended to multi-modal propagation. Finally, the proposed FET equivalent structure (*i.e.* with transconductance and drain-source resistance) is classically met, e.g. for NGD applications [43].

Based on the EM cavity theory, the 3-D structure introduced in Fig. 3(b) is equivalent to the circuit shown in Fig. 5(a). The model is relying on the developments proposed in [45] for the modeling of EM cavities. The principles were applied in [46] with electrical simulator tools to the simulation of multi-dimensional mode stirred reverberation chambers. The access ports with subscripts k=1,2 are connected to transformers T$_k$(n_k:1) which are specified by transform ratio, n_k. The considered propagative mode is equivalent to the R$_d$L$_d$C$_d$-parallel network mounted in parallel. The resonance frequency is given by:

$$\omega_0\approx\pi c\sqrt{\left(\frac{m_x}{L_x}\right)^2+\left(\frac{m_y}{L_y}\right)^2+\left(\frac{m_z}{L_z}\right)^2}. \quad (20)$$

with $m_{x,y,z}$ are integers corresponding to the propagation modes, TE/TM(m_x,m_y,m_z). The equivalent circuit of equalized cavity proposed in Fig. 3(c) is depicted in Fig. 5(b). It is composed of the cavity equivalent circuit (Fig. 5(a)) in cascade with the NGD active cell. This later one consists of an RLC-series network mounted in parallel connected between the gate and source of an FET with drain and source connected by a shunt resistance R_m.

Based on the principle of the BP NGD equalization explained in the previous section, the design method of NGD solution in function of the 3-D EM cavity will be described in the following subsection via S-matrix modelling of equalized circuit presented in Fig. 5(b).

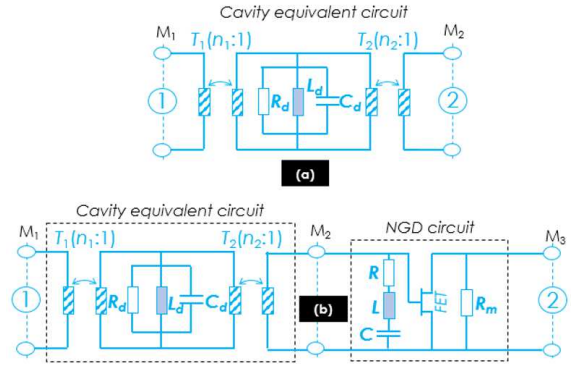

Fig. 5. Equivalent circuits of (a) simple and (b) NGD equalized cavity.

B. S-Matrix Model of the NGD Equalized Circuit

By denoting the Laplace variable, $s=j\omega$, the two-port S-matrix model, $\left[S^{eq}(s)\right]$, of the NGD equalized circuit presented in Fig. 5(b) can be determined from the ABCD matrix, $\left[ABCD^{eq}(s)\right]$. Because of the cascade configuration, we have:

$$\left[ABCD^{eq}(s)\right]=\left[ABCD^{EMI}(s)\right]\times\left[ABCD^{N}(s)\right] \quad (21)$$

where:

- The cavity equivalent circuit ABCD matrix is written as:

$$\left[ABCD^{EMI}(s)\right]=\begin{bmatrix}\dfrac{1}{n_1 n_2} & 0\\ \dfrac{n_1 Y_d(s)}{n_2} & n_1 n_2\end{bmatrix} \quad (22)$$

- The NGD equivalent circuit ABCD matrix is given by:

$$\left[ABCD^{N}(s)\right]=\frac{-1}{g_m}\begin{bmatrix}\dfrac{R_m+R_{ds}}{R_m R_{ds}} & 1\\ \dfrac{R_m+R_{ds}}{R_m R_{ds} Z(s)} & \dfrac{1}{Z(s)}\end{bmatrix} \quad (23)$$

where:

$$\begin{cases} Y_d(s)=\dfrac{1}{R_d}+\dfrac{1}{L_d s}+C_d s \\ Z(s)=R+Ls+1/(Cs)\end{cases}. \quad (24)$$

By means of ABCD-to-S matrix transform, with the reference impedance, R_0=50 Ω, we have equalized cavity S-matrix elements:

$$S_{11}^{eq}(s)=\frac{Z(s)-n_1^2 R_0\left[n_2^2+Y_d(s)Z(s)\right]}{Z(s)+n_1^2 R_0\left[n_2^2+Y_d(s)Z(s)\right]} \quad (25)$$

$$S_{21}^{eq}(s)=\frac{-2n_1 n_2 R_0 g_m R_{ds} Z(s)}{\left[R_m R_{ds}+R_0(R_m+R_{ds})\right]\left\{Z(s)+n_1^2 R_0\left[n_2^2+Y_d(s)Z(s)\right]\right\}} \quad (26)$$

$$S_{22}^{eq}(s)=\frac{R_m R_{ds}-R_0(R_m+R_{ds})}{R_m R_{ds}+R_0(R_m+R_{ds})}. \quad (27)$$

C. Design Equation of the NGD Circuit Equalizer

As introduced in Section II, the initial data of the problem corresponds to the 3-D EM cavity parameters. The solution of the problem is the NGD circuit design. The next paragraphs develop how the NGD design equations are established.

1) Equalization Hypothetical Equation

The design equation of the NGD circuit equalizer are the expression of the parameters R_m, R, L and C in function of the EM cavity ones R_d, L_d and C_d.

$$C_d=1/(L_d\omega_0^2). \quad (28)$$

The elaboration of the equations is based on the hypotheses:

- the NGD center frequency should coincide with the cavity resonance frequency:

$$\omega_0=\omega_n^N=1/\sqrt{LC}. \quad (29)$$

by inverting this equation, we can write the capacitor value:

$$C=1/(L\omega_0^2). \quad (30)$$

- The equalized cavity input/output reflection and transmission coefficients obey equations (10) and (11).

2) Synthesis Equations of R and L

The magnitude of the transmission coefficient given in equation (26) is equal to:

$$S_{21}^{eq}(\omega)=\frac{2n_1 n_2 R_0 g_m R_{ds}\sqrt{R^2\omega^2+L^2(\omega^2-\omega_0^2)^2}}{\left[R_m R_{ds}+R_0(R_m+R_{ds})\right]\sqrt{X^2(\omega)+Y^2(\omega)}} \quad (31)$$

with:

$$X(\omega)=\omega(\omega_0^2-\omega^2)\left[n_1^2 R_0 R R_d+L\omega_0^2 L_d(R_0+R_d)\right] \quad (32)$$

$$Y(\omega)=\begin{cases}\omega^2\left[L_d R_d R+n_1^2 R_0\left[L_d R+R_d(2L+n_2^2 L_d)\right]\right]\\ -R_0 R_d L n_1^2(\omega_0^4+\omega^4)\end{cases}. \quad (33)$$

The Taylor series limited expansion of this transmission coefficient $\left[S_{21}^{eq}(\omega)\right]^2$ with respect to variable, $\omega\approx\omega_0$, enables to write:

$$\left[\tilde{S}_{21}^{eq}(\omega)\right]^2\approx\left[S_{21}^{eq}(\omega_0)\right]^2+\psi(R,L,\omega_0)(\omega^2-\omega_0^2)+O(\omega^3) \quad (34)$$

where:

$$S_{21}^{eq}(\omega_0)=\frac{2n_1 n_2 R_0 R_m R_d g_m R_{ds}}{\left[R_m R_{ds}+R_0(R_m+R_{ds})\right]\left[R_d R+n_1^2 R_0(R+n_2^2 R_d)\right]} \quad (35)$$

$$\psi(\omega_0)=\frac{16n_1^4 n_2^2 R_0^3 R_m^2 R_d^3 g_m^2 R_{ds}^2(\psi_4\omega_0^4+\psi_2\omega_0^2-n_1^2 R_0 R_d R^4)}{L_d^2\omega_0^4\left[R_m R_{ds}+R_0(R_m+R_{ds})\right]^2\left[R_d R+n_1^2 R_0(R+n_2^2 R_d)\right]^4} \quad (36)$$

with:

$$\begin{cases}\psi_2=2n_1^2 n_2^2 R_0 R_d R^2 L_d L\\ \psi_4=n_2^2 L^2 L_d^2\left[n_1^2 R_0(2n_2^2 R_d+R)+2R_d R\right]\end{cases}. \quad (37)$$

Consequently, equation (11) can be rewritten as:

$$\begin{cases}S_{21}^{eq}(\omega_0)\approx 1\\ \psi(R,L,\omega_0)\approx 0\end{cases}. \quad (38)$$

The solutions of this equation system are the NGD equalizer parameters expressed as:

$$R=\frac{n_1^2 n_2^2 R_0 R_d}{n_1\left[\dfrac{2n_2 R_0 R_d g_m R_{ds}}{R_m R_{ds}+R_0(R_m+R_{ds})}-n_1\right]-R_d} \quad (39)$$

$$L=\frac{n_1 R^2\sqrt{R_0 R_d}\begin{cases}\sqrt{2\left[R_d R+n_1^2 R_0(n_2^2 R_d+R)\right]}\\ -n_1 n_2\sqrt{R_0 R_d}\end{cases}}{n_2 L_d\omega_0^2\left[2R_d R+n_1^2 R_0(n_2^2 R_d+2R)\right]}. \quad (40)$$

The existence condition of the resistance related to the FET parameters is defined by:

$$g_m\geq g_{m_{\min}}=\frac{(R_0 n_1^2+R_d)\left[R_m R_{ds}+R_0(R_m+R_{ds})\right]}{2n_1 n_2 R_0 R_m R_d R_{ds}}. \quad (41)$$

3) Synthesis Equations of R_m

The resistance R_m serve to the NGD circuit output matching. In function of the matching constraint r (for example better than -10 dB), it can be determined from equation:

$$S_{22}^{eq}(\omega)=r. \quad (42)$$

It yields the equation:

$$R_m=\begin{cases}\dfrac{(1-r)R_0 R_{ds}}{r(R_{ds}+R_0)+R_{ds}-R_0}\\ \dfrac{(1+r)R_0 R_{ds}}{r(R_{ds}+R_0)+R_{ds}-R_0}\end{cases}. \quad (43)$$

To verify the feasibility of the developed equalization method, a proof-of-concept will be examined in the next section.

IV. Proof-of-Concept of Cavity Resonance Equalization

The present section deals with the validations of the developed NGD equalization method for minimizing the effect of 3-D EM cavity resonance. The numerical applications in both frequency and time domains were performed in Matlab environment.

A. Frequency Domain Validation of the EM Cavity NGD Equalization Method

After the proof-of-concept, description, validation results based on transmission coefficient and GD are presented in this subsection.

1) Proof-of-Concept Description

The proof-of-concept circuits of the 2-D lower resonance frequency of the rectangular cavity designed in the ADS® schematic environment are presented in Fig. 6. Following works in [45-46], the proof-of-concept physical and electrical parameters are addressed in Table I. The resonance behavior of this structure was reported in [22]. The interested reader may find the equivalence between cavity parameters definition and equivalent circuit design, developed through Kron's methodology, in [22]. The cavity is assumed to be constituted by Copper enclosure and wire antennas. The NGD equalizer parameters were calculated from equations (39), (40) and (43) by taking r=-10 dB. The minimal value of FET transconductance to realize the equalization is $g_{m,min}$=22 mS.

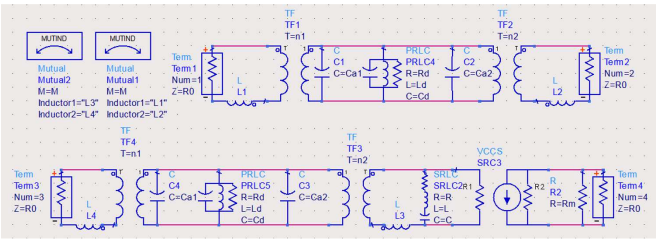

Fig. 6. Simulated schematic of cavity and cavity+NGD equivalent circuits.

TABLE I
CONSIDERED PARAMETERS OF THE 3-D EM CAVITY

Type	Description	Name	Value
Geometrical	Length	L_x	42 cm
		d_1	3 cm
		d_2	2 cm
	Width	L_y	28 cm
	Height	L_z	3.8 cm
Cavity equivalent circuit	Resonance frequency	$f_0=f_{1,1,0}$	646 MHz
	Resistance	R_d	47 kΩ
	Inductance	L_d	0.93 nH
	Capacitance	C_d	65.5 pF
	Transformer coefficient ratio	n_1	1
		n_2	0.7
NGD circuit	FET	g_m	70 mS
		R_{ds}	200 Ω
	Resistance	R_m	185 Ω
		R	11 Ω
	Inductance	L	5.98 nF
	Capacitance	C	10 pF

2) Frequency Domain Demonstration of Equalized Cavity Resonance Responses

The present frequency domain analysis is based on the S-parameter simulated from 0.4 GHz to 1 GHz. The feasibility of the NGD equalization can be understood with resonant ("EMI" in red dashed line) and equalized ("Eq." in black solid line) of S_{21} and GD plotted in Figs. 7. The bandpass NGD function is shown by the dotted blue curves with NGD center frequency $f_n=f_0$ and NGD value about -0.85 ns.

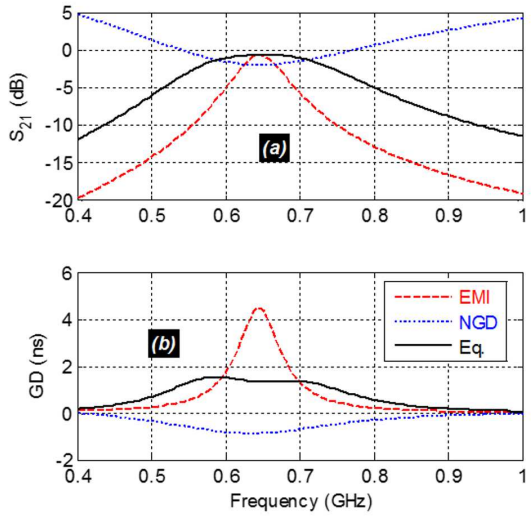

Fig. 7. EMI (dashed red line), NGD (dotted blue line) and equalized (solid black line): (a) magnitude and (b) GD frequency responses.

The EM cavity resonance effect manifests with concave response around f_0 with peak $S_{21}(f_0)$=-0.72 dB and $GD(f_0)$=4.47 ns. The dispersion due to the resonance over the bandwidth BW=0.1 GHz can be estimated with the ranges of attenuation $\Delta S_{21}\approx$-6 dB and $\Delta GD\approx$4 ns. Thanks to the introduction of NGD circuit, a significant reduction of S_{21} and GD fastnesses into ΔS_{21NGD}<-1 dB and ΔGD_{NGD}<0.3 ns can be observed respectively with black curves of Fig. 7(a) and Fig. 7(b), respectively.

3) Equalized Results with Parametric Analysis with Respect to the Cavity Equivalent Circuit Parameters

In addition to the previous validation, for the better understanding on the NGD equalization method robustness, parametric analyses were performed with different values of R_d={0.1 to 100 kΩ}, L_d={0.9 to 1 nH} and C_d={50 to 90 pF}. Mapping S_{21} and GD results in the frequency band 0.5 to 0.8 GHz with respect to, R_d in logarithmic scale, is introduced in Figs. 8. It can be emphasized that the equalization effect is still confirmed by the improvement of flatness of (ΔS_{21EMI}, ΔGD_{EMI}) compared to ($\Delta S_{21eq.}$, $\Delta GD_{eq.}$). This flatness reduction robustness is also verified with the other parametric analyses with respect to L_d and C_d as seen in Figs. 9 and in Figs. 10, respectively. However, in these two last cases of parametric analyses the cavity resonance frequencies are intentionally shifted while the NGD center frequency was kept f_n=646 MHz. More rigorous illustration of the resonance cavity NGD equalization method is discussed in the following subsection by considering a Gaussian pulse modulated with sine wave signal carrier with f_0.

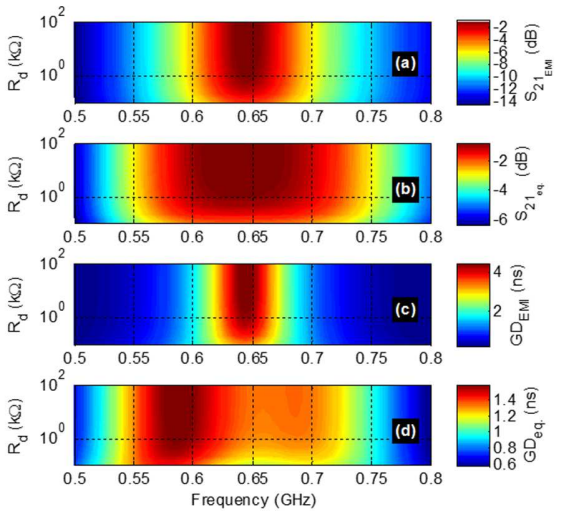

Fig. 8. Mapping of (a) EMI and (b) equalized circuit transmission coefficients, and (c) EMI and (d) equalized circuit GD vs R_d.

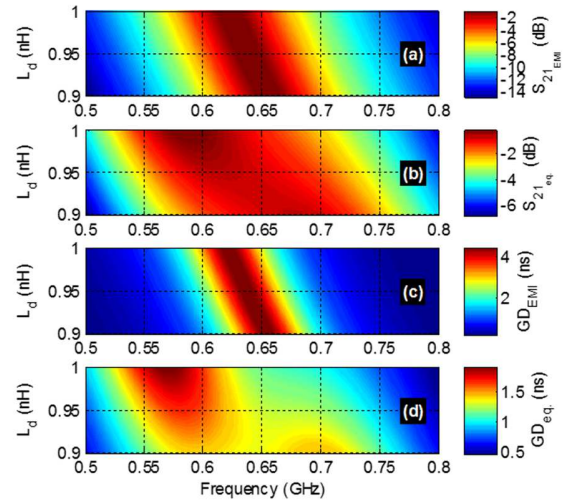

Fig. 9. Mapping of (a) EMI and (b) equalized circuit transmission coefficients, and (c) EMI and (d) equalized circuit GD vs L_d.

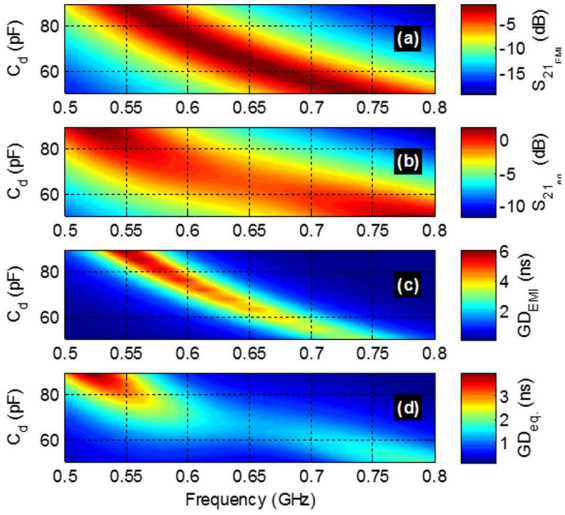

Fig. 10. Mapping of (a) EMI and (b) equalized circuit transmission coefficients, and (c) EMI and (d) equalized circuit GD vs C_d.

B. Time Domain Results of Bandpass NGD Equalization

A single pulse signal presenting a Gaussian waveform with about 17 ns time width and 1 V amplitude was assumed as a test signal. The time domain analysis was performed in 40 ns time window with 0.25 ns time step. This input signal was injected to the cavity and equalized cavity circuits by taking into account the source and load impedances R_0=50 Ω. Therefore, we obtain the transient input ("v_{in}"), resonance circuit ("v_{EMI}"), and equalized signal ("$v_{eq.}$"), results respectively depicted in Figs. 11(a-c). The corresponding signal envelopes ("Env.") are shown in Figs. 12. Fig. 11 and Fig. 12 rigorously confirm the effectiveness of the bandpass NGD function equalization in the time-domain.

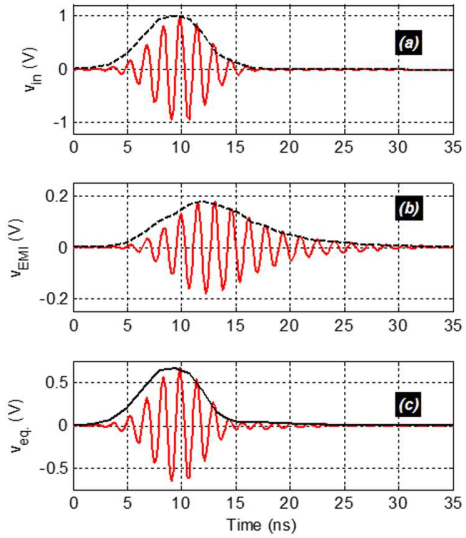

Fig. 11. Transient plot results of (a) input, (b) EMI and (c) equalized signals.

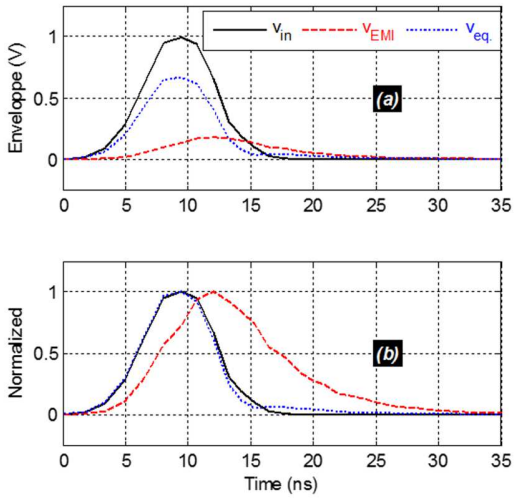

Fig. 12. (a) Natural and (b) normalized envelope (env.) plot results of input, EMI and equalized signals.

As expected in the previous frequency analysis, the EMI signal v_{EMI} of Fig. 11(b) illustrates the time spreading due to the resonance from the cavity. The coherence between the input and output signals can be assessed with correlation coefficient comparisons [47]. This correlation can be estimated with discrete signals, for example, giving the number of sampling,

$k_{\max}$, and the time step, $\Delta t = t_{\max} / k_{\max}$. We can denote the sampled signals and the associated average value, respectively:

$$\begin{cases} v_{\kappa}(k) = v_{\kappa}(k\Delta t) \\ v_{\kappa,ave} = \sum_{k=1}^{k_{\max}} v_{\kappa}(k) / k_{\max} \end{cases} \quad (44)$$

where the subscript, $\kappa=\{in, EMI, eq.\}$. Accordingly, we have considered the correlation coefficient, x_{κ}, between the initial and signal envelope subscripted, $\kappa=\{EMI, eq.\}$:

$$x_{\kappa} = \frac{\sum_{k=1}^{k_{\max}} \left[v_{in}(k) - v_{in,ave} \right] \left[v_{\kappa}(k) - v_{\kappa,ave} \right]}{\sqrt{\sum_{k=1}^{k_{\max}} \left\{ \left[v_{in}(k) - v_{in,ave} \right] \left[v_{\kappa}(k) - v_{\kappa,ave} \right] \right\}^2}} . \quad (45)$$

The calculated cross correlation between the input and EMI distorted signals plotted in Figs. 12 was equal to x_{EMI}=66.2%. After the NGD equalization, the cross correlation was widely improved to $x_{eq.}$=99.5%.

V. Conclusion

An original equalization method of 3-D EM cavity EMI and resonance effect by using bandpass NGD function is initiated. The developed NGD method presents a considerable simplicity. The method is based on the S-matrix modelling of the cavity and NGD equivalent circuit. The equalization analytical mechanism as a function of the NGD key parameters is described. The NGD function synthesis approach is established as a function of the EMI effect.

The relevance of bandpass NGD equalization is illustrated with both frequency and time domain applications. A cavity proof-of-concept corresponding to a rectangular EM enclosure was performed. The frequency and time domain analyses were realized by considering equivalent circuits simulated in a commercial tool environment. The NGD equalization feasibility was quantified with improvement of transmission coefficient and GD flatness around the resonance frequency. Furthermore, time domain analyses rigorously confirm the feasibility of the EMI equalization effect. The distorted signal envelope was clearly improved with the correlation coefficient increasing from 66.2% to more than 99.5%.

As ongoing research, the proposed NGD EMI equalization method will be validated by measurement and also applied to multiple EMI source effect reduction. In the future, the developed NGD equalization method can be potentially exploited to correct complex EMIs as in the reverberation chamber (RC) [48, 49]. From both simulation and experimental point of views, the proposed methodology (noise mitigation through NGD equalization) might also be helpful when dealing with EMC issues involving printed circuit boards (PCBs), as for numerical [49-51] EMC susceptibility and/or emission [50] problems.

References

[1] Z. Zhang and C. L. Law, "Short-Delay Multipath Mitigation Technique Based on Virtual Multipath," IEEE Ant. Wireless Propag. Lett., Vol. 4, Sept. 2005, pp. 344-348.

[2] K. J. Kim, M. D. Renzo, H. Liu, P. V. Orlik and H. V. Poor, "Performance Analysis of Distributed Single Carrier Systems With Distributed Cyclic Delay Diversity," IEEE Trans. Comm, vol. 65, no. 12, Dec. 2017, pp. 5514-5528.

[3] C. Gao and X. Cao, "Effect of Group Delay on Channel Estimation Performance in OFDM System," in Proc. 2009 First International Conference on Information Science and Engineering, Nanjing, China, 26-28 Dec. 2009, pp. 2618-2621.

[4] P. M. Mariappan, D. R. Raghavan, S. H. E. A. Aleem and A. F. Zobaa, "Effects of electromagnetic interference on the functional usage of medical equipment by 2G/3G/4G cellular phones: A review," Journal of Advanced Research, vol. 7, no. 5, Sept. 2016, pp. 727-738.

[5] K. Ishida, T. Fujioka, T. Endo, R. Hosokawa, T. Fujisaki, R. Yoshino and M. Hirose, "Evaluation of Electromagnetic Fields in a Hospital for Safe Use of Electronic Medical Equipment," Journal of medical systems, vol. 40, no. 3, Mar. 2016, pp. 46/1-11.

[6] E. Hanada, K. Kodama, K. Takano, Y. Watanabe and Y. Nose, "Possible electromagnetic interference with electronic medical equipment by radio waves coming from outside the hospital," J. Med. Syst., vol. 25, no. 4, Aug. 2001, pp. 257-267.

[7] R. Azaro, S. Caorsi, M. Cosso, G. M. Costini, M. Donelli, R. Ene, G. L. Gragnani and M. Pastorino, "A semi-analytical approach for the evaluation of radiated immunity on a printed-circuit board in metallic enclosures," Microwave and Optical Technology Letters, vol. 27, no. 3, Nov. 2000, pp. 204-207.

[8] M. Bertocco and A. Sona, "Analysis and Mitigation of EMC Effects of Electric Resonances in Circuits", in Proc. 2018 Int. Symp. On EMC, EMC Europe 2018, Amsterdam, The Netherlands, 27-30 Aug. 2018, pp. 930-934.

[9] X. T. I. Ngu, A. Nothofer, D. W. P. Thomas and C. Christopoulos, "A Complete Model for Simulating Magnitude and Phase of Emissions from a DUT Placed Inside a GTEM Cell," IEEE Trans. Electromagn. Compat., vol. 49, no. 2, May 2007, pp. 285-293.

[10] D. Hansen, D. Ristau, W. A. Radasky and K. S. Smith, "Sources of problems in the GTEM structure and recommended solutions," in Proc. Symposium on Electromagnetic Compatibility, 1996, Santa Clara, CA, USA, 19-23 Aug. 1996, pp. 48-51.

[11] Z. L. Wang, O. Wada, Y. Toyota and R. Koga, "Convergence acceleration and accuracy improvement in power bus impedance calculation with a fast algorithm using cavity modes," IEEE Trans. Electromagn. Compat., vol. 47, no. 1, pp. 2-9, Feb. 2005.

[12] M. Luo and K.-M. Huang, "Prediction of the Electromagnetic Field in Metallic Enclosures Using Artificial Neural Networks," Progress In Electromagnetics Research, vol. 116, pp. 171-184, 2011.

[13] V. Rajamani, C. F. Bunting, M. D. Deshpande and Z. A. Khan, "Validation of Modal / MoM in Shielding Effectiveness Studies of Rectangular enclosures with Apertures," IEEE Trans. Electromagn. Compat., vol. 48, no. 2, May 2006, pp 348-353.

[14] J. M. Lu, Y. S. Li and M. S. Zhang, "An efficient SPICE-compatible cavity resonant model for microstrip lines," IEEE Trans. Compon. Package. Manuf. Technol, vol. 1, no. 4, Apr. 2011, pp. 574-585.

[15] https://www.3ds.com/products-services/simulia/products/cst-studio-suite/, accessed 2020.

[16] https://www.ansys.com/products/electronics/ansys-hfss, accessed 2019.

[17] https://altairhyperworks.com/product/FEKO/Applications-Antenna-Design, accessed 2020.

[18] https://www.keysight.com/us/en/assets/7018-02343/brochures/5990-4819.pdf, accessed 2020.

[19] EM/EMC Simulation Software, https://www.emcos.com/?product-types=em-simulation-software, accessed 2020.

[20] M. P. Robinson, T. M. Benson, C. Christopoulos, J. F. Dawson, M. D. Ganley, A. C. Marvin, S. J. Porter and D. W. P. Thomas, "Analytical formulation of the shielding effectiveness of enclosures with apertures," IEEE Trans. Electromagn. Compat., vol. 40, no. 3, Aug. 1998, pp 240-248.

[21] T. Yang, and J. L. Volakis, "Coupling onto Wires Enclosed in Cavities with Apertures," Electromagnetics, vol. 25, no. 7-8, 2005, pp. 655-678.

[22] S. Leman, B. Demoulin, O. Maurice, M. Cauterman and P. Hoffmann, "New approaches in Electromagnetic Compatibility: Use of the circuit approach to solve large EMC problems," C. R. Physique, vol. 10, no. 1, Jan. 2009, pp. 70–82.

[23] M. Backstrom, T. Martin, J. Loren, "Analytical model for boundary estimates of shielding effectiveness of complex resonant cavities," in proc. IEEE Internat. Symp. On EMC, 2003 EMC'03, Istanbul, Turkey, 2003.

[24] F. Gronwald, "Method of moment analysis of a dipole antenna within a rectangular cavity," in proc. IEEE Internat. Symp. On EMC, 2003 EMC'03, Istanbul, Turkey, 2003.

[25] F. Gronwald, "Calculation of mutual antenna coupling within rectangular enclosures," IEEE Trans. Electromagn. Compat., vol. 47, no. 4, Nov. 2005, pp. 1021-1025.

[26] C. Lange and M. Leone, "Broadband circuit model for electromagnetic-interference analysis in metallic enclosures," IEEE Trans. Electromagn. Compat., vol. 60, no. 2, Apr. 2018, pp. 368-375.

[27] C. Lange, P. Konrad, and M. Leone, "Experimental validation of a broadband circuit model for electromagnetic-interference analysis in metallic enclosures," 2018 IEEE Symposium on Electromagnetic Compatibility, Signal Integrity and Power Integrity (EMC, SI & PI), Long Beach, CA, 2018, pp. 571-576.

[28] X.-C. Nie and N. Yuan, "Accurate Modeling of Monopole Antennas in Shielded Enclosures with Apertures," Progress In Electromagnetics Research, vol. 79, 2008, pp. 251-262.

[29] N. J. Nešić, and N. S. Dončov, "Shielding Effectiveness Estimation by using Monopole-receiving Antenna and Comparison with Dipole Antenna," Frequenz, vol. 70, no. 5-6, May 2016, pp. 191–201.

[30] C.-Q. Jiao and H.-Z. Zhu, "Resonance suppression and electromagnetic shielding effectiveness improvement of an apertured rectangular cavity by using wall losses," Chinese Physics B, vol. 22, no. 8, Aug. 2013, pp. 084101/1-6.

[31] F. Z. Mahmood, Y. Toyota and K. Iokibe, "Lossy resonators for suppressing power-bus resonance of printed circuit boards," IEEE Electromagnetic Compatibility Magazine, vol. 3, no. 1, 1st Quarter 2014, pp. 65-69.

[32] S. Shahparnia and O. M. Ramahi, "Electromagnetic interference (EMI) reduction from printed circuit boards (PCB) using electromagnetic bandgap structures," IEEE Trans. Electromagn. Compat., vol. 64, no. 4, Nov. 2004, pp. 580-587.

[33] K.-P. Ahn, R. Ishikawa and K. Honjo, "Group Delay Equalized UWB InGaP/GaAs HBT MMIC Amplifier using Negative Group Delay Circuits," IEEE Trans. Microw. Theory Techn., vol. 57, no. 9, Sept. 2009, pp. 2139-2147.

[34] B. Ravelo, A. Perennec and M. Le Roy, "Synthesis of frequency-independent phase shifters using negative group delay active circuit", Int. J. RF and Microwave Computer-Aided Engineering (RFMiCAE), vol. 21, no. 1, Jan. 2011, pp. 17-24.

[35] C. D. Broomfield and J. K. A. Everard, "Broadband negative group delay networks for compensation of microwave oscillators and filters," Electronics Letters, vol. 36, no. 23, pp. 1931-1933, 9 Nov. 2000,

[36] H. Takahashi, R. Inohara, K. Nishimura and M. Usami, "Expansion of bandwidth of tunable dispersion compensator based on ring resonators utilizing negative group delay," Journal of Lightwave Technology, vol. 24, no. 6, pp. 2276-2286, June 2006.

[37] L. Qiu, L. Wu, W. Yin and J. Mao, "A filter with equal-ripple negative group delay," in Proc. of 2018 IEEE Radio and Wireless Symposium (RWS), Anaheim, CA, 15-18 Jan. 2018, pp. 263-266

[38] B. Ravelo, "Neutralization of LC- and RC-Effects with Left-Handed and NGD Circuits," Advanced Electromagnetics (AEM), vol. 2, no. 1, Sept. 2013, pp. 73-84.

[39] L.-F. Qiu, L.-S. Wu, W.-Y. Yin, and J.-F. Mao, "Absorptive bandstop filter with prescribed negative group delay and bandwidth," IEEE Microw. Wireless Compon. Lett., vol. 27, no. 7, pp. 639-641, Jul. 2017.

[40] G. Liu and J. Xu, "Compact transmission-type negative group delay circuit with low attenuation," Electron. Lett., vol. 53, no. 7, pp. 476-478, Mar. 2017.

[41] T. Shao, Z. Wang, S. Fang, H. Liu, and S. Fu, "A compact transmission line self-matched negative group delay microwave circuit," IEEE Access, vol. 5, Oct. 2017, pp. 22836-22843.

[42] Z. Wang, Y. Cao, T. Shao, S. Fang and Y. Liu, "A Negative Group Delay Microwave Circuit Based on Signal Interference Techniques," IEEE Microw. Wireless Compon. Lett., vol. 28, no. 4, Apr. 2018, pp. 290-292.

[43] B. Ravelo, A. Perennec, M. Le Roy and Y. Boucher, "Active Microwave Circuit with Negative Group Delay", IEEE Microwave and Wireless Components Letters, vol. 17, no. 12, Dec. 2007, pp. 861-863.

[44] B. Ravelo, "Similitude between the NGD function and filter gain behaviours," Int. J. Circ. Theor. Appl., vol. 42, no. 10, Oct. 2014, pp. 1016-1032.

[45] G. L. Ragan, "Microwave transmission circuits," McGraw-Hill Ed., New-York, chapter 10, 1948.

[46] H. Moussa, S. Baranowski, M. Cauterman and B. Demoulin, "Simulation of a 2D cavity under Qucs," in Proc. Symposium on Embedded EMC, 2EMC, 25-27 Oct. 2007, Rouen, France, pp. 1-7.

[47] R. L. Mickelson and G. W. Swenson, "A comparison of two correlation schemes," IEEE Trans. Instrum. Meas., vol. 40, no. 5, Oct. 1991, pp. 816-819.

[48] M. Magdowski, S. V. Tkachenko, and R. Vick, "Coupling of stochastic electromagnetic fields to a transmission line in a reverberation chamber," IEEE Trans. Electromagn. Compat., vol. 53, no. 2, May 2011, pp. 308-317.

[49] H. Tarhini, M. El Haffar, C. Guiffaut, G. Andrieu, A. Reineix, B. Pecqueux and J. C. Joly "Susceptibility of printed circuit boards in complex electromagnetic environment," in Proc. 2008 International Symposium on Electromagnetic Compatibility - EMC Europe, Hamburg, Germany, 8-12 Sept. 2008, pp. 1-4.

[50] X. Li and Z. Du, "Combined FEM-reaction method for EMS analysis of a PCB in a low-Q enclosure," in Proc. 2017 IEEE 5th International Symposium on Electromagnetic Compatibility (EMC-Beijing), Beijing, China, 28-31 Oct. 2017, pp. 1-4.

[51] S. Leman, R. Omarouayache, F. Hoëppe and A. Piche, "Prediction of Electronic Unit Radiated Emissions from Both PCB Near Field and Shielding Enclosure Characterization," in Proc. 2019 ESA Workshop on Aerospace EMC (Aerospace EMC), Budapest, Hungary, 20-22 May 2019, pp. 1-6.